

## Photocatalytic H<sub>2</sub> production over inverse opal TiO<sub>2</sub> catalysts

*Roberto Fiorenza,<sup>a\*</sup> Marianna Bellardita,<sup>b</sup> Salvatore Scirè,<sup>a</sup> and Leonardo Palmisano<sup>b</sup>*

*<sup>a</sup> Dip. Scienze Chimiche, Università di Catania, Viale A. Doria 6, 95125 Catania (Italy).*

*<sup>b</sup> DEIM, Università di Palermo, Viale delle Scienze, 90128 Palermo (Italy).*

\* Corresponding author: *e-mail address:* rfiorenza@unict.it

**Keywords:** Photocatalysis, Titanium dioxide, Water splitting, Photonic effect, Porous structures

### **Abstract**

The influence of BiVO<sub>4</sub> and CuO on the chemico-physical properties of TiO<sub>2</sub>-based systems is reported. The performances of these systems were investigated in the photocatalytic H<sub>2</sub> production under both UV and solar light irradiation. The characterization data pointed out that the obtained TiO<sub>2</sub> samples have highly porous inverse opal structures with interconnected macropores. Inverse opal TiO<sub>2</sub> exhibited higher activity in the H<sub>2</sub> production than the commercial TiO<sub>2</sub> both under UV and solar light irradiation due to the peculiar porosity that allows photons to enter inside the photocatalyst. A further improvement in terms of photoactivity was verified by addition of increasing amounts of BiVO<sub>4</sub>. On the contrary for the inverse opal TiO<sub>2</sub>-CuO composites a small CuO content was found to be the optimal one. In fact, due to surface segregation effects, a higher amount of CuO can partially keep the light radiation away from TiO<sub>2</sub> surface active sites, thus decreasing drastically the absorption of photons. The combination of the benefits of the highly ordered porous TiO<sub>2</sub> structure and the presence of BiVO<sub>4</sub> or small amounts of CuO can represent a promising strategy towards efficient photocatalytic H<sub>2</sub> production.

## 1. Introduction

The environmental harms and the energy crisis are amongst the main concerns of modern society. The progressive depletion of fossil fuel reserves and the environmental pollution caused by the combustion of them make hydrogen more attractive as clean, storable and environmentally friendly fuel [1,2]. However, being hydrogen an energy carrier, it is necessary developing sustainable and green methods for its production. Since Fujishima and Honda reported the photoelectrochemical evolution of H<sub>2</sub> on the TiO<sub>2</sub> electrode in 1972 [3], the photoactivity of TiO<sub>2</sub>-based materials was intensively investigated both for the photocatalytic water splitting and degradation of toxic organics. Titanium dioxide exhibits some advantages as its stability, low cost, and no toxicity [4,5]. To improve the photocatalytic efficiency of TiO<sub>2</sub>, much effort has been made to modify the size, the morphology, the electronic structure and the preparation method. In particular, mesoporous structures have been studied due to their large accessible surface area and well defined uniform pore size and intrinsic connectivity, which favour an efficient charge carrier transfer and mass flow of the reactants [6,7]. In this contest, three-dimensional inverse opal structures prepared by template strategy were recently investigated as a promising class of photocatalysts with peculiar structure and macro-mesoporosity [8-10]. In these materials the particular porous backbone acts in fact as a photon trap, taking advantage also of the scattering effects [11,12]. An important issue for active materials in the photocatalytic reactions is, in fact, the light absorption property which is strongly correlated with the conversion efficiency of photons to electrons.

Another approach to enhance the photoactivity is the combination of TiO<sub>2</sub> with noble metals (Pt, Ag or Au) or other oxides [13-15].

Non-noble metals co-catalysts such as cobalt or copper have also shown good photocatalytic performance in the water splitting reaction [16-18] with the advantage of lower cost compared to noble metals.

In this contest BiVO<sub>4</sub> is an attractive material for solar water splitting due to its small band gap (2.4 eV) which enables a wide absorption in the portion of the visible spectrum [19,20]. The good stability and the suitable valence band energy position to oxidize water are, in addition, key features either on its own or coupled with TiO<sub>2</sub> [21,22]. Furthermore, the combination of a highly ordered three dimensional macroporous titania (3DOM TiO<sub>2</sub>) with BiVO<sub>4</sub> has achieved good results in the photodegradation of Rhodamine B under visible light irradiation [23].

On these basis, we studied the combination of structural (synthesis of inverse opal  $\text{TiO}_2$  with a highly ordered porous framework) and chemical modifications of  $\text{TiO}_2$  (addition of different amounts of  $\text{CuO}$  and  $\text{BiVO}_4$  to the inverse opal  $\text{TiO}_2$ ) with the aim to investigate how these changes can influence the  $\text{H}_2$  production under both UV and solar light irradiation. From a practical point of view the solar water splitting is a promising strategy to produce  $\text{H}_2$  without using fossil fuel playing a key role towards a sustainable hydrogen-based energy economy.

## **2. Experimental**

### ***2.1. Catalyst preparation***

Inverse opal (I.O.)  $\text{TiO}_2$  was synthesized via a templating strategy using polystyrene (PS) spheres, obtained by free-surfactant emulsion polymerization, according to the method previously reported in the literature [8,9,23]. Briefly, after the formation of the PS spheres the following steps consisted of an infiltration procedure with a solution of titanium isopropoxide, drying for 24 h and calcining at  $550^\circ\text{C}$  for 12 h (heating ramp of  $2^\circ\text{C}/\text{min}$ ) leading to the formation of the inverse opal  $\text{TiO}_2$  structure through the removal of the PS template.

The I.O.  $\text{TiO}_2$ - $\text{CuO}$  composites were prepared by adding a proper amount of the metal salt precursor (copper(II) chloride) to the titanium isopropoxide-sol used for the infiltration.

The I.O.  $\text{TiO}_2$ - $\text{BiVO}_4$  composites were prepared by the hydrothermal method by mixing stoichiometric amounts of  $\text{Bi}(\text{NO}_3)_3 \cdot 5\text{H}_2\text{O}$  and  $\text{NH}_4\text{VO}_3$  with an ethylene glycol-water solution, stirring until the obtainment of a clear solution [23,24]. Subsequently, after the addition of the I.O.  $\text{TiO}_2$  powder, the mixture was sonicated for 15 min, stirred for 1 h and heated at  $160^\circ\text{C}$  for 24 h inside a Teflon autoclave. Washing with distilled water, drying at  $100^\circ\text{C}$  for 24 h and calcination at  $300^\circ\text{C}$  for 3 h (ramp of  $2^\circ\text{C}/\text{min}$ ) were the final steps to synthesize the inverse opal  $\text{TiO}_2$ - $\text{BiVO}_4$  systems.

All  $\text{TiO}_2$ -composites were prepared with different nominal concentrations of copper oxide and bismuth vanadate (from 1 to 25% weight percentages).

A commercial sample of  $\text{TiO}_2$  anatase (Sigma Aldrich prod. Nos. 637254) was used for the photocatalytic activity comparisons.

### ***2.2. Catalyst characterization***

The structure and the morphology of the samples were evaluated by scanning electron microscopy (SEM) using a Jeol JSM-7500F instrument, and by transmission electron microscopy (TEM) using a Jeol JEM 2100F operating at 200 kV.

The X-ray powder diffraction (XRD) measurements were carried out with a PANalytical X'pertPro X-ray diffractometer using a Cu K $\alpha$  radiation. The JCPDS Data File was utilized to compare the detected diffraction peaks of the samples.

The BET surface area of the composites were estimated by the nitrogen adsorption-desorption measurements with a Micromeritics Tristar 3000. Samples were outgassed at 120°C overnight before the measurements.

The surface properties were investigated with a K-Alpha<sup>TM</sup>+ X-ray photoelectron spectrometer. The C (1s) peak at 285.8 eV (coming from the adventitious carbon) was used as reference for the X-ray photoelectron spectroscopy (XPS) analyses.

Ultraviolet-Visible-Diffuse Reflectance Spectroscopy (UV-Vis DRS) was performed by Perkin Elmer Lambda 35 UV-visible spectrometer, BaSO<sub>4</sub> was used as the reference.

### ***2.3. Photocatalytic activity experiments***

Hydrogen generation by photocatalytic reforming of aqueous ethanol solution was performed in a home-made Pyrex jacketed reactor thermostated at 30°C. The evolution of H<sub>2</sub> was quantified by analyzing the effluent gases with an online gas chromatograph equipped with a packed column (Carboxen 1000) and thermal conductivity detector using Argon as carrier gas. Specifically, the catalyst (25 mg) was placed inside the photo-reactor with 45 mL of deionized water and 5 ml of ethanol used as sacrificial agent, under stirring. The suspension was purged with an argon flow for at least 1 h before irradiation in order to remove dissolved air. Then it was irradiated for 5 h by using a UV 100 W Hg lamp (Blak-Ray B 100A, 365 nm) or a special lamp designed for sunlight simulation (Osram Ultra Vitalux 300W).

## **3. Results and discussion**

**Figure 1** shows H<sub>2</sub> evolution under UV and solar light irradiation in the presence of the investigated TiO<sub>2</sub> based systems. Under UV irradiation the bare I.O. TiO<sub>2</sub> (red line) showed a higher H<sub>2</sub> production compared to commercial TiO<sub>2</sub> anatase (black curve) (**Figures 1A-B**). The presence of BiVO<sub>4</sub> (**Figure 1A**) led to a moderate increase of H<sub>2</sub>

production, which was more relevant for the samples with the highest amount (I.O. TiO<sub>2</sub>-10% BiVO<sub>4</sub> and I.O. TiO<sub>2</sub>-25% BiVO<sub>4</sub>). On the contrary the addition of CuO (Figure 1B) had a negative effect on the performance, even at a low copper amount.

Under solar light irradiation (Figures 1C-D) the I.O. TiO<sub>2</sub> exhibited a much higher activity (about 5 times) compared to commercial TiO<sub>2</sub>. Also in this case concentrations of BiVO<sub>4</sub> higher than 10 wt.% resulted in a further increase of the hydrogen production, with the I.O. TiO<sub>2</sub>-25% BiVO<sub>4</sub> sample exhibiting the best performance (Figure 1C violet line). On the contrary for the I.O. TiO<sub>2</sub>-CuO composites (Figure 1D) only the samples with small amounts of CuO (1-3 wt. %) had a better activity with respect to I.O. TiO<sub>2</sub>.

The higher photoactivity of I.O. TiO<sub>2</sub> compared to commercial TiO<sub>2</sub> anatase cannot be ascribed to a different TiO<sub>2</sub> phase. In fact, I.O. TiO<sub>2</sub> also adopts the anatase phase, as shown by XRD reported in Figure 2 (signals at  $2\theta = 25.3^\circ, 37.8^\circ, 48.0^\circ, 54.0^\circ$  and  $55.1^\circ$  [25,26]). SEM and TEM images (Figure 3) showed an ordered macroporous structure of I.O. TiO<sub>2</sub> with interconnections between the pores. Single porous domains are present inside the material, in agreement with the morphology of other inverse opals prepared with the template method [8,9,23]. This macroporosity can be claimed to explain the increased photoactivity, as it can favour the mass transfer and consequently the reduction of H<sup>+</sup> ions on the surface of TiO<sub>2</sub> by the photogenerated electrons. In addition, the ordered network can increase the optical path length of incident light radiation caused by the multiple reflection inside the macroporous structure [27,28], generating at the end, more electron-hole pairs to split water.

To better understand the photocatalytic activity trend and the changes in the chemico-physical properties of the inverse opal TiO<sub>2</sub> due to the presence of BiVO<sub>4</sub> or CuO, the structural, optical and surface properties of the composites were evaluated by various techniques (XRD, surface area determination, UV-VIS DRS and XPS).

Regarding the structural properties, it must be highlighted that no substantial changes in the inverse opal TiO<sub>2</sub> morphology was observed in the presence of CuO or BiVO<sub>4</sub>. The XRD patterns of I.O. TiO<sub>2</sub>-BiVO<sub>4</sub> (Figure 2A) show that only the samples with the 10 and 25 wt.% of BiVO<sub>4</sub> display both signals of TiO<sub>2</sub> (anatase) and BiVO<sub>4</sub> (monoclinic scheelite [29,30]). Similarly, also for the I.O. TiO<sub>2</sub>-CuO series (Figure 3B) the catalysts with a high amount of copper oxide (I.O. TiO<sub>2</sub>-10%CuO and I.O. TiO<sub>2</sub>-25%CuO) exhibited both TiO<sub>2</sub> (anatase) and copper(II)oxide (monoclinic CuO at  $2\theta = 35.7^\circ$  and  $38.9^\circ$  [31,32]) signals. No peak associated to copper(I) oxide was detected, according to

the thermal treatment used (calcination at 550°C) [32,33]. The lack of signals of the BiVO<sub>4</sub> and CuO, when their amount was lower than 10 wt.%, was presumably due to the low content and/or high dispersion (small particle size) of the host oxide in I.O. TiO<sub>2</sub> composites.

The average crystallites size of TiO<sub>2</sub> in the investigated composites, determined by applying the Scherrer formula using the (1 0 1) anatase diffraction peak ( $2\theta = 25.3^\circ$ ), is reported in the Table 1. In the I.O. TiO<sub>2</sub>-BiVO<sub>4</sub> system, the TiO<sub>2</sub> crystal size varied slightly and progressively with the amount of bismuth vanadate from 25 to 29 nm. In the I.O. TiO<sub>2</sub>-CuO composites the TiO<sub>2</sub> crystal sizes slightly decreased for low amounts of copper oxide (from 25 to 20 nm). This can be ascribed to the introduction of CuO nanoparticles in the crystal lattice of I.O. TiO<sub>2</sub> (the copper precursor was added together with titanium isopropoxide, before the thermal treatment), thus inhibiting the TiO<sub>2</sub> aggregation [34]. This process was favoured when the amount of copper oxide was low. Consequently, a slight increase in the BET surface area values was detected for the I.O. TiO<sub>2</sub>-CuO samples with a CuO amount < 5 wt.% (Table 1), whereas no significant variation was found in the I.O. TiO<sub>2</sub>-BiVO<sub>4</sub> series. The macroporous structure of the catalysts was further confirmed by type II N<sub>2</sub> adsorption-desorption isotherms found for all of the investigated samples [35].

To evaluate the optical properties of the samples, their UV-Vis DRS spectra and band gap energies,  $E_g$ , determined by the modified Kubelka–Munk function,  $[F(R_\infty')/hv]^{1/2}$ , are reported in Figure 4 and Table 1 respectively.

The I.O. TiO<sub>2</sub>-BiVO<sub>4</sub> system (Figure 4A) showed an enhancement of absorption in the visible region by increasing the amount of bismuth vanadate. Consequently a decrease of the band-gap energy was observed (Table 1). It is noteworthy that another absorption feature at about 400 nm was detected in the samples with higher BiVO<sub>4</sub> amounts, more evident for the TiO<sub>2</sub>-25%BiVO<sub>4</sub> catalyst. As it can be seen in the inset of Figure 4A, plotting  $[F(R_\infty')/hv]^{1/2}$  versus the energy of the exciting light for TiO<sub>2</sub>-25%BiVO<sub>4</sub>, two contributes were found, one at 3.19 eV, due to I.O. TiO<sub>2</sub> and another at 2.40 eV, due to monoclinic BiVO<sub>4</sub> [36,37]. In accordance with the literature, the presence of these two features suggests the formation of an efficient heterojunction between the I.O. TiO<sub>2</sub> and the BiVO<sub>4</sub> [38].

The TiO<sub>2</sub> band edges of the I.O. TiO<sub>2</sub>-CuO samples are all shifted towards the visible region (Figure 4B), indicating that additional energy levels were created by the Cu ions in the band gap of TiO<sub>2</sub> [32,34], as confirmed by the presence of a midgap band located

above the valence band in the sample containing high CuO amounts (inset of Figure 4B). Moreover a small decrease (0.05-0.09 eV) in the TiO<sub>2</sub> band-gap energies can be observed (Table 1). As reported in the literature, CuO electrons can give excitation from the valence band to the exciton level (< 730 nm), d-d transition of Cu<sup>2+</sup> giving absorption in the 600-800 nm range. These features are ascribed to the CuO nanoparticles, embedded inside the skeleton of TiO<sub>2</sub> [34,39]. It has been reported [40] that the presence of Cu(II) causes a shift of the valence band edge towards less positive values, and consequently a decrease of the band gap.

To investigate the oxidation states and the surface composition of involved species, XPS measurements of the I.O. TiO<sub>2</sub> composites were carried out and the results summarized in Table 2.

Regarding the I.O. TiO<sub>2</sub>-BiVO<sub>4</sub> composites, the signals detected in the vanadium and in the bismuth zone are characteristic of V(V) and Bi(III) [41,42], whereas no substantial shift compared to I.O. TiO<sub>2</sub> was measured in the Ti and O XPS regions. Noteworthy the surface atomic concentrations of V and Bi in the I.O. TiO<sub>2</sub>-3% BiVO<sub>4</sub> are very low (Table 2). Probably (according to XRD data) the use of a little amount of precursor salts is not sufficient to form the bismuth vanadate oxide at the interface of TiO<sub>2</sub>.

The binding energies values of the Cu 2p zone indicate that copper is mostly present on the surface of I.O. TiO<sub>2</sub> as Cu<sup>2+</sup> [43,44]. In this case, the I.O. TiO<sub>2</sub>-25%CuO exhibited a 0.6 eV shift at higher binding energy compared to I.O. TiO<sub>2</sub> both in Ti and O regions. In accordance with the literature [45] this shift can be ascribed to the electron transfer from TiO<sub>2</sub> to CuO (also in agreement to DRS measurements) favoured when the amount of copper oxide was high. By comparing the atomic percentages of Bi<sup>3+</sup> and Cu<sup>2+</sup>, it can be seen that BiVO<sub>4</sub> is dispersed within the TiO<sub>2</sub> matrix, whilst CuO is mostly present on the surface.

The above reported results indicate that the combination of structural (obtainment of an inverse opal backbone) and chemical (presence BiVO<sub>4</sub> or CuO) modifications of TiO<sub>2</sub> is capable of enhancing the photocatalytic H<sub>2</sub> production. In particular, the presence of a macroporous structure such as that of I.O. TiO<sub>2</sub> largely improves the absorption of photons, increasing the path length and the migration rate of electron-hole pairs towards the surface. Consequently the reduction of H<sup>+</sup> ions on the surface of TiO<sub>2</sub> by the photogenerated electrons is favoured [27,28]. This well agrees with the observed higher photoactivity of I.O. TiO<sub>2</sub> compared to commercial TiO<sub>2</sub>. This photoactivity is

further increased in the presence of BiVO<sub>4</sub>. The sample with the highest BiVO<sub>4</sub> content, I.O. TiO<sub>2</sub>-25%BiVO<sub>4</sub>, exhibited the best performance both under UV than solar irradiation. Due to the small band-gap of BiVO<sub>4</sub>, the produced high-energy electrons in the bare BiVO<sub>4</sub> relax easily from the conduction (CB) to the valence band (VB) in a remarkably short period, with obvious energy loss, leading to an inefficient charge separation. The coupling of BiVO<sub>4</sub> with TiO<sub>2</sub> leads to an increase of photocatalytic performances. As reported in the literature, in fact, BiVO<sub>4</sub> can be considered as a light sensitizer for TiO<sub>2</sub>. In particular, a generally accepted mechanism considers that under a suitable light irradiation ( $\lambda_{\text{excitation}} \leq 510\text{-}530$  nm) the electrons of the valence band of BiVO<sub>4</sub> are firstly excited to the conduction band of BiVO<sub>4</sub>, leaving holes behind, and after that these photogenerated electrons are transferred to the CB of TiO<sub>2</sub> [22,46]. The formation of an efficient heterojunction between TiO<sub>2</sub> and BiVO<sub>4</sub> is a key factor to explain the enhanced photoactivity. On the basis of XRD, XPS and DRS measurements we found that the heterojunction was favoured only for high amount of BiVO<sub>4</sub> (>10 wt%). This is in good agreement with the results of Zalfani et al. [23], who investigated the photodegradation of Rhodamine B under visible light irradiation over BiVO<sub>4</sub>-TiO<sub>2</sub> catalysts.

Figure 5 depicts the band positions versus the Normal Hydrogen Electrode (NHE) of the different semiconductors according to the literature data [39,47-50]. In the TiO<sub>2</sub>-BiVO<sub>4</sub> systems (Fig. 5A), electrons can be transferred from BiVO<sub>4</sub> to TiO<sub>2</sub> because the conduction band of BiVO<sub>4</sub> is more negative than that of TiO<sub>2</sub>, whilst holes, due to the more positive valence band of TiO<sub>2</sub>, can move in the opposite direction allowing a very efficient charge separation and an improvement of the photocatalytic activity. On the contrary, in the TiO<sub>2</sub>-CuO samples (Fig. 5B), both holes and electrons will transfer and accumulate on CuO, giving rise also to some extent of recombination, because the conduction band of CuO is more positive than that of TiO<sub>2</sub>, making consequently the junction not very efficient under UV irradiation. Consequently the bare I.O. TiO<sub>2</sub> sample showed to be more active than the TiO<sub>2</sub>-CuO samples. However, from an electrochemical point of view, CuO could favour H<sub>2</sub> formation only if its conduction band edge was more negative than the H<sup>+</sup>/H<sub>2</sub> potential. In accord to Yu *et al.* [39], when the CuO amount is not very high (1 and 3%, in this paper), particle size is small and, due to quantum size effect, the valence and conduction band edges shift toward more positive and more negative values, respectively. In particular the conduction band edge can become more negative than the H<sup>+</sup>/H<sub>2</sub> potential, allowing H<sub>2</sub> evolution. This finding



could explain the highest activity of the I.O. TiO<sub>2</sub>-1%CuO and I.O. TiO<sub>2</sub>-3%CuO samples with respect to the other doped samples. In addition, some authors [32,47,48] explain the CuO efficiency toward H<sub>2</sub> production by considering that electron excess on CuO under irradiation causes a negative shift of the Fermi level of the oxide, enabling H<sup>+</sup> reduction.

It is worth noting that according to literature [51-53], H<sub>2</sub> formation can derive both from H<sub>2</sub>O splitting and ethanol reforming, while the presence of CO<sub>2</sub> detected during the photocatalytic tests can be related to the mineralization of the organic compound acting as a sacrificial agent.

Contrarily to what observed under UV irradiation, I.O.TiO<sub>2</sub>-CuO composites with the smallest amounts of CuO (< 5 wt.%) showed to be more photoactive under solar light irradiation with respect to I.O. TiO<sub>2</sub>. It is not easy to explain this apparent contradictory behaviour. A tentative explanation could be provided by considering (i) that only a smaller fraction of efficient UV photons are present in a 300 W lamp simulating solar light (with respect to the high number of photons deriving from a 100 W UV lamp which could give rise to a levelling effect in the accumulation/recombination of pairs), (ii) that a beneficial effect could be due to the presence of CuO which can absorb in the visible range with the occurrence of d-d transition in Cu<sup>2+</sup> species (as detected by DRS measurements), thus favouring the accumulation of electrons in the CB of CuO [39, 48].

XRD and DRS results suggest that the incorporation of small amounts of CuO in the inverse opal TiO<sub>2</sub> allowed the occurrence of a charge tunneling through the interface barrier between the two oxides. CuO could act as a co-catalyst, offering the reduction sites for H<sub>2</sub> production (Figure 5B). The presence of a high CuO loading appeared to be detrimental because the oxide acted as a recombination site between the charge carriers and the unfavorable band position due to the particle size increase. Moreover, high amount of CuO segregated on the TiO<sub>2</sub> surface (see XPS results) can inhibit light absorption by TiO<sub>2</sub> [54,55].

## 5. Conclusions

Inverse opal TiO<sub>2</sub>-BiVO<sub>4</sub> and TiO<sub>2</sub>-CuO samples have been synthesized, characterized and tested in the photocatalytic water splitting under both UV and solar

light irradiation. The influence of the addition of different amounts of  $\text{BiVO}_4$  and  $\text{CuO}$  was evaluated both in terms of chemico-physical properties and photocatalytic activity.

The peculiar porous backbone of inverse opal  $\text{TiO}_2$  led to a high light absorption inside the materials and allowed to exploit the photonic effects, resulting in a higher activity compared to the commercial  $\text{TiO}_2$  both under UV and solar light irradiation. A further improvement in terms of  $\text{H}_2$  production was also verified by addition of an increasing amount of  $\text{BiVO}_4$ . On the contrary, for the I.O.  $\text{TiO}_2$ - $\text{CuO}$  composites, small copper oxide content was found to be optimal. In fact, due to surface segregation of copper, a higher amount of  $\text{CuO}$  can decrease the absorption of photon energy on  $\text{TiO}_2$  surface due to the coverage of the  $\text{TiO}_2$  active sites.

Combination of  $\text{TiO}_2$  structural modifications as the synthesis of inverse opal materials, and chemical modifications as the addition of a host  $\text{BiVO}_4$  or  $\text{CuO}$  can be a promising strategy to enhance the  $\text{H}_2$  production by photocatalytic water splitting.

### Acknowledgments

We thank Prof. Bao-Lian Su, director of Laboratory of Inorganic Materials Chemistry (CMI), University of Namur (Belgium), for the materials characterization facilities.

### References

- [1] D.Y.C. Leung, X. Fu, C. Wang, M. Ni, M.K.H. Leung, X. Wang, X. Fu, *ChemSusChem* 3 (2010) 68.
- [2] X. Chen, S. Shen, L. Guo, S.S. Mao *Chem. Rev.* 110 (2010) 6503.
- [3] A. Fujishima, K. Honda, *Nature* 238 (1972) 37.
- [4] V. Augugliaro, M. Bellardita, V. Loddo, G. Palmisano, L. Palmisano, S. Yurdak, *J. Photoch. Photobio. C* 13 (2012) 224.
- [5] M. Ni, M.K.H. Leung, D.Y.C. Leung, K. Sumathy. *Renew. Sustainable Energy Rev.* 11 (2007) 401.
- [6] J.H. Pan, X. Zhao, W.I. Lee, *Chem. Eng. J.* 170 (2011) 363.
- [7] Y. Ye, C. Jo, I. Jeong, J. Lee, *Nanoscale* 5 (2013) 4584.
- [8] L. Xin, X. Liu, *RSC Adv.* 5 (2015) 71547.
- [9] M. Wu, J. Liu, J. Jin, C. Wang, S. Huang, Z. Deng, B.L. Su, *Appl. Catal., B: Environ.* 150-151 (2014) 411.
- [10] J. Ginter, A. Kisielewska, K. Spilarewicz-Stanek, M. Cichomski, D. Batory, I. Piwonsk, *Micropor. Mesopor. Mat.* 225 (2016) 580.
- [11] F. Sordello, V. Maurino, C. Minero *J. Mater. Chem.* 21 (2011), 19144.
- [12] G. Liao, S. Chen, X. Quan, H. Chen, Y. Zhang, *Environ Sci. Technol.* 44 (2010) 3481.
- [13] A. Kudo, Y. Miseki *Chem. Soc. Rev.* 38 (2009) 253.
- [14] M. Bellardita, E.I. García-López, G. Marci, L. Palmisano, *Int. J. Hydrog. Energy* 41 (2016) 5934.

- [15] R. Fiorenza, M. Bellardita, L. D'Urso, G. Compagnini, L. Palmisano, S. Scire` Catalysis (2016) 121.
- [16] Z. Yan, H. Wu, A. Han, X. Yu, P. Du, *Int. J. Hydrog. Energy* 39 (2014) 13353.
- [17] S.J.A. Moniz, J. Tang *ChemCatChem* 7 (2015) 1659.
- [18] V. Gombac, L. Sordelli, T. Montini, J.J. Delgado, A. Adamski, G. Adami, M. Cargnello, S. Bernal, P. Fornasiero, *J. Phys. Chem. A* 114 (2010) 3916.
- [19] Z. He, Y. Shi, C. Gao, L. Wen, J. Chen, S. Song, *J. Phys. Chem. C* 118 (2014) 389-398.
- [20] T.W. Kim, K.S. Choi, *Science* 343 (2014) 990.
- [21] Z. Jian, S. Huang, Y. Cao, Y. Zhang, *Photochem Photobiol* 92 (2016) 363.
- [22] M. Xie, X. Fu, L. Jing, P. Luan, Y. Feng, H. Fu, *Adv. Energy Mater.* 4 (2014) 1300995.
- [23] M. Zalfani, Z.Y. Hu, W. Yu, M. Mahdouani, R. Bourguiga, M. Wu, Y. Li, B. van G. Van Tendeloo, Y. Djaoued, B.L. Su, *Appl. Catal. B Environ.* 205 (2017) 121.
- [24] Y. Guo, X. Yang, F. Ma, K. Li, L. Xu, X. Yuan, Y. Guo, *Appl. Surf. Sci.* 256 (2010) 2215.
- [25] C. Su, B.Y. Hong, C.M. Tseng, *Catal. Today* 96 (2004) 119.
- [26] G. Marcì, V. Augugliaro, M.J. López-Muñoz, C. Martín, L. Palmisano, V. Rives, M. Schiavello, R.J.D. Tilley, A.M. Venezia, *J. Phys. Chem. B.* 105 (2001) 1026.
- [27] H. Xu, X. Chen, S.X. Ouyang, T. Kako, J.H. Ye, *J. Phys. Chem. C* 116 (2012) 3833.
- [28] J.I.L. Chen, E. Loso, N. Ebrahim, G.A. Ozin, *J. Am. Chem. Soc.* 130 (2008) 5420.
- [29] A.K. Bhattacharya, K.K. Mallick, A. Hartridge, *Mater. Lett.* 30 (1997) 7.
- [30] C.M. Huang, G.T. Pan, P.Y. Peng, T.C.K. Yang, *J. Mol. Catal. A: Chem.* 327 (2010) 38.
- [31] Z.N. Kayani, M. Umer, S. Riaz, S. Naseem, *J. Electron. Mater.* 44 (2015) 3704.
- [32] J. Bandara, C.P.K. Udawatta, C.S.K. Rajapakse, *Photochem. Photobiol. Sci.* 4 (2005) 857.
- [33] Z.N. Kayani, M. Umer, S. Riaz, S. Naseem, *J. Electron. Mater.* 44 (2015) 3704.
- [34] R. Yang, L. Yang, T. Tao, F. Ma, M. Xu, Z. Zhang, *Appl. Surf. Sci.* 288 (2014) 363.
- [35] H. Yan, C.F. Blanford, B.T. Holland, W.H. Smyrl, A. Stein, *Chem. Mater.* 12 (2000) 1134.
- [36] A. Kudo, K. Omori, H. Kato, *J. Am. Chem. Soc.* 121 (1999) 11459.
- [37] Y. Hu, D. Li, Y. Zheng, W. Chen, Y. He, Y. Shao, X. Fu, G. Xiao, *Appl. Catal. B* 104 (2011) 30.
- [38] S. Umrao, S. Abraham, F. Theil, S. Pandey, V. Ciobota, P.K. Shukla, C.J Rupp, S. Chakraborty, R. Ahuja, J. Popp, B. Dietzek, A. Srivastava, *RSC Adv.* 4 (2014) 59890.
- [39] J. Yu, Y. Hai, M. Jaroniec, *J. Colloid Inter. Sci.* 357 (2011) 223.
- [40] A. Di Paola, E. García-López, G. Marcì, C. Martín, L. Palmisano, V. Rives, A.M. Venezia, *Appl. Catal. B* 48 (2004) 223.
- [41] N. Myung, S. Ham, S. Choi, Y. Chae, W. Kim, Y.J. Jeon, K. Paeng, W. Chanmanee, N.R. de Tacconi, K. Rajeshwar, *J. Phys. Chem. C* 115 (2011), 7793.
- [42] L. Dong, S. Guo, S. Zhu, D. Xu, L. Zhang, M. Huo, X. Yang, *Catal. Commun.* 16 (2011) 250.
- [43] H. Yu, H. Irie, K. Hashimoto, *J. Am. Chem. Soc.* 132 (2010) 6898.
- [44] H. Irie, K. Kamiya, T. Shibamura, S. Miura, D.A. Tryk, T. Yokoyama, K. Hashimoto, *J. Chem. Phys. C* 113 (2009) 10761.

- [45] B.F. Xin, P. Wang, D.D. Ding, J. Liu, Z.Y. Ren, H.G. Fu, *Appl. Surf. Sci.* 254 (2008) 2569.
- [46] J. Sun, X. Li, Q. Zhao, M.O. Tadé, S. Liu, *J. Mater. Chem. A* 3 (2015) 21655.
- [47] H. Hou, M. Shang, F. Gao, L. Wang, Q. Liu, J. Zheng, Z. Yang, W. Yang *ACS Appl. Mater. Interfaces* 8 (2016) 20128.
- [48] S. Xu, J. Ng, A.J. Du, J. Liu, D.D. Sun, *Int. J. Hydrog. Energy* 36 (2011) 6538.
- [49] S. Moniz, S.A. Shevlin, D. Martin, Z. Guo, J. Tang, *Energy Environ. Sci.* 8 (2015) 731.
- [50] J. Resasco, H. Zhang, N. Kornienko, N. Becknell, H. Lee, J. Guo, A.L. Briseno, P. Yang, *ACS Cent. Sci.* 2 (2016) 80.
- [51] A. Patsoura, D.I. Kondarides, X.E. Verykios, *Catal. Today* 124 (2007) 94.
- [52] C.R. López, E. Pulido Melián, J.A. Ortega Méndez, D.E. Santiago, J.M. Doña Rodríguez, O. González Díaz, *J. Photochem. Photobiol. A* 312 (2015) 45.
- [53] T. Puangpetch, T. Sreethawong, S. Yoshikawa, S. Chavadej, *J. Mol. Catal. A: Chem.* 312 (2009) 97.
- [54] S. Xu, D.D. Sun, *Int. J. Hydrog. Energy* 34 (2009) 6096.
- [55] L. Delannoy, G. Thrimurthulu, P.S. Reddy, C. Méthivier, J. Nelayah, B.M. Reddy, C. Ricolleaudand, C. Louisa, *Phys.Chem.Chem.Phys.* 16 (2014) 26514.

**Table 1** Crystallite size (calculated by Scherrer equation), BET Surface area ( $S_{BET}$ ) and Band-gap energy ( $E_g$ ) for the investigated I.O.  $TiO_2$  samples.

Catalysts	Crystallite size (nm)	$S_{BET}$ ( $m^2 g^{-1}$ )	$E_g$ (eV)
$TiO_2$	25.4	28.0	3.23
$TiO_2$ -1% $BiVO_4$	25.1	28.3	3.19
$TiO_2$ -3% $BiVO_4$	25.6	30.3	3.18
$TiO_2$ -5% $BiVO_4$	26.2	29.7	3.17
$TiO_2$ -10% $BiVO_4$	28.1	28.1	3.19
$TiO_2$ -25% $BiVO_4$	29.3	27.3	3.17
$TiO_2$ -1% $CuO$	22.8	32.7	3.25
$TiO_2$ -3% $CuO$	21.9	31.4	3.19
$TiO_2$ -5% $CuO$	20.0	33.0	3.16 2.04*
$TiO_2$ -10% $CuO$	24.2	28.2	3.18 2.10*
$TiO_2$ -25% $CuO$	25.6	29.5	3.14 2.06*

\* Midgap value.

**Table 2** XPS binding energies and atomic composition of the investigated I.O.  $TiO_2$  catalysts.

Catalysts	Ti 2p (eV)	O 1s (eV)	V 2p (eV)	Bi 4f (eV)	Cu 2p (eV)	Ti (at%)	O (at%)	Bi (at%)	V (at%)	Cu (at%)
$TiO_2$	458.8 464.8	529.8 531.6	-	-	-	30.5	55.7	-	-	-
$TiO_2$ -3% $BiVO_4$	458.9 464.9	529.6 532.4	516.0 523.6	low intensity	-	32.8	58.8	0.01	0.04	-
$TiO_2$ -25% $BiVO_4$	458.5 464.5	530.2 531.2	517.0 524.5	159.5 164.5	-	28.6	51.5	1.7	0.9	-
$TiO_2$ -3% $CuO$	458.8 464.8	530.3 531.9	-	-	933.2 953.0	25.3	59.1	-	-	1.2
$TiO_2$ -25% $CuO$	459.4 465.4	530.8 532.6	-	-	933.9 953.0	27.6	52.2	-	-	9.9

**Captions to figures**

- Fig. 1** Photocatalytic H<sub>2</sub> production at 30°C: (A) Inverse Opal TiO<sub>2</sub>-BiVO<sub>4</sub> and (B) Inverse Opal TiO<sub>2</sub>-CuO composites under UV irradiation; (C) Inverse Opal TiO<sub>2</sub>-BiVO<sub>4</sub> and (D) Inverse Opal TiO<sub>2</sub>-CuO under solar light irradiation.
- Fig. 2** XRD patterns of Inverse Opal TiO<sub>2</sub>-BiVO<sub>4</sub> (A) and Inverse Opal TiO<sub>2</sub>-CuO (B) systems.
- Fig. 3** SEM (A) and TEM (C) images of Inverse Opal TiO<sub>2</sub> sample at different magnifications.
- Fig. 4** UV-Vis Diffuse reflectance spectra of (A) Inverse Opal TiO<sub>2</sub>-BiVO<sub>4</sub> and (B) Inverse Opal TiO<sub>2</sub>-CuO composites.
- Fig. 5** Possible photocatalytic mechanism of H<sub>2</sub> generation over (A) Inverse Opal TiO<sub>2</sub>-BiVO<sub>4</sub> and (B) Inverse Opal TiO<sub>2</sub>-CuO composites.

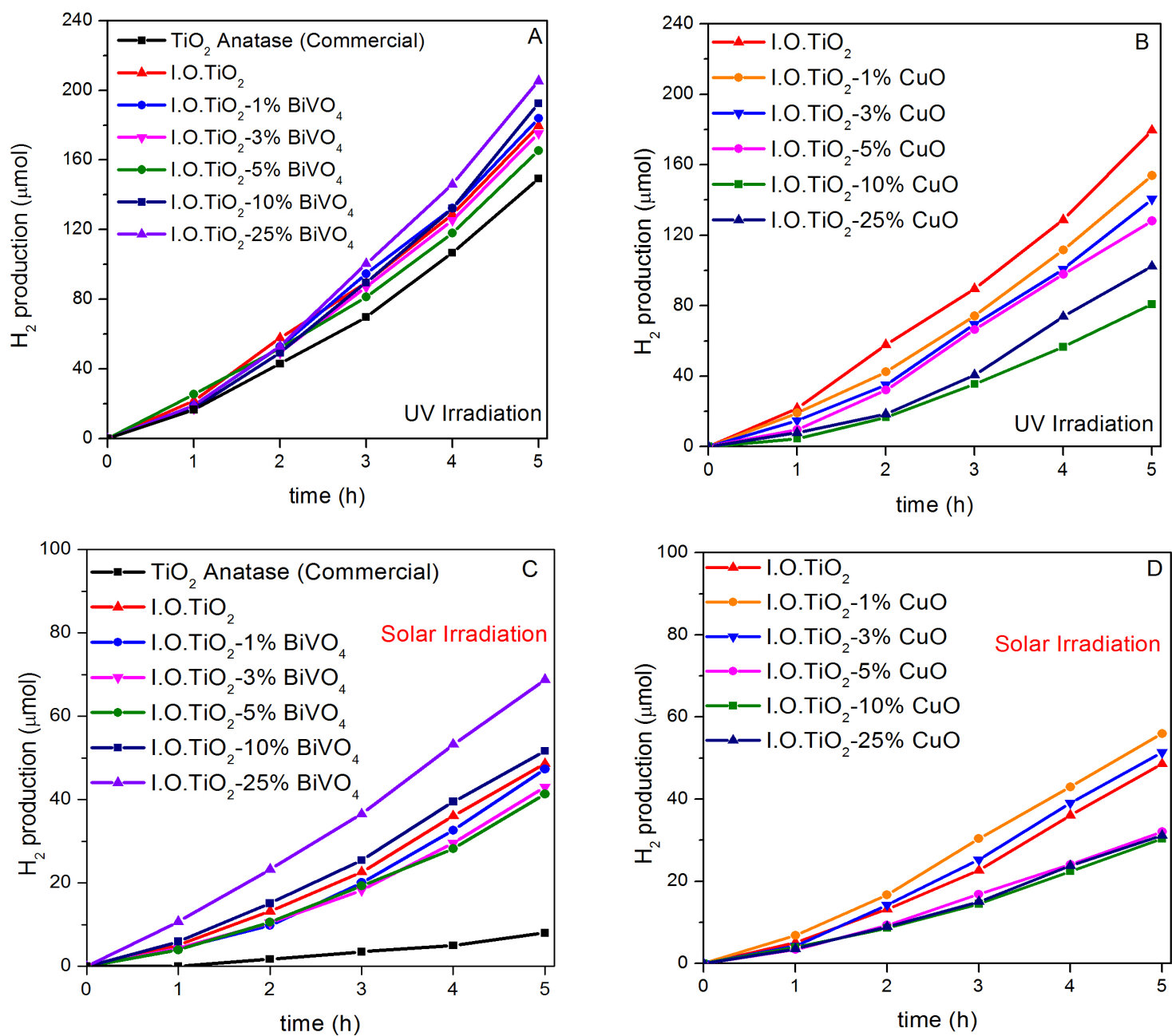
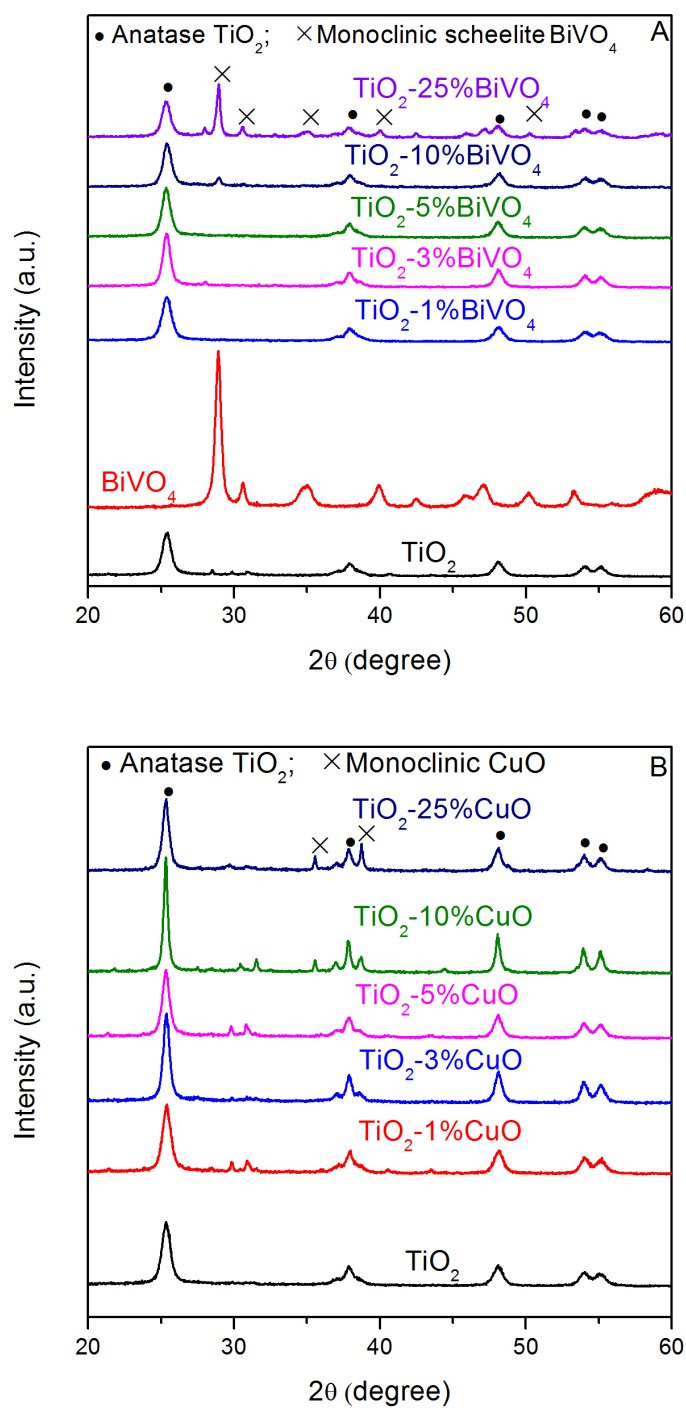
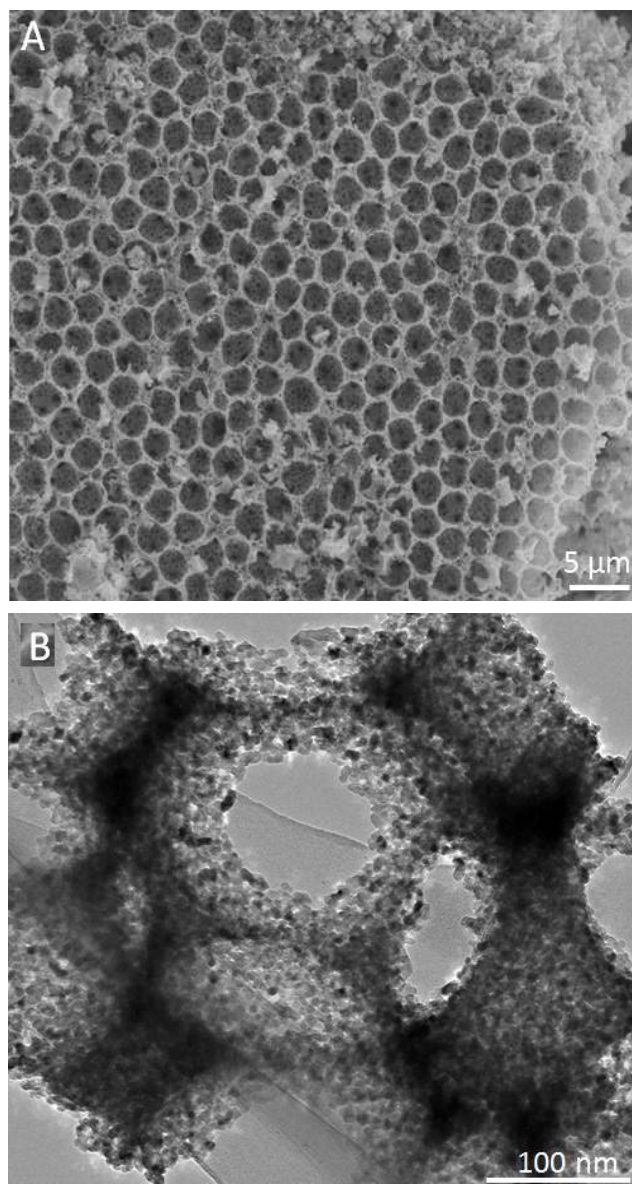


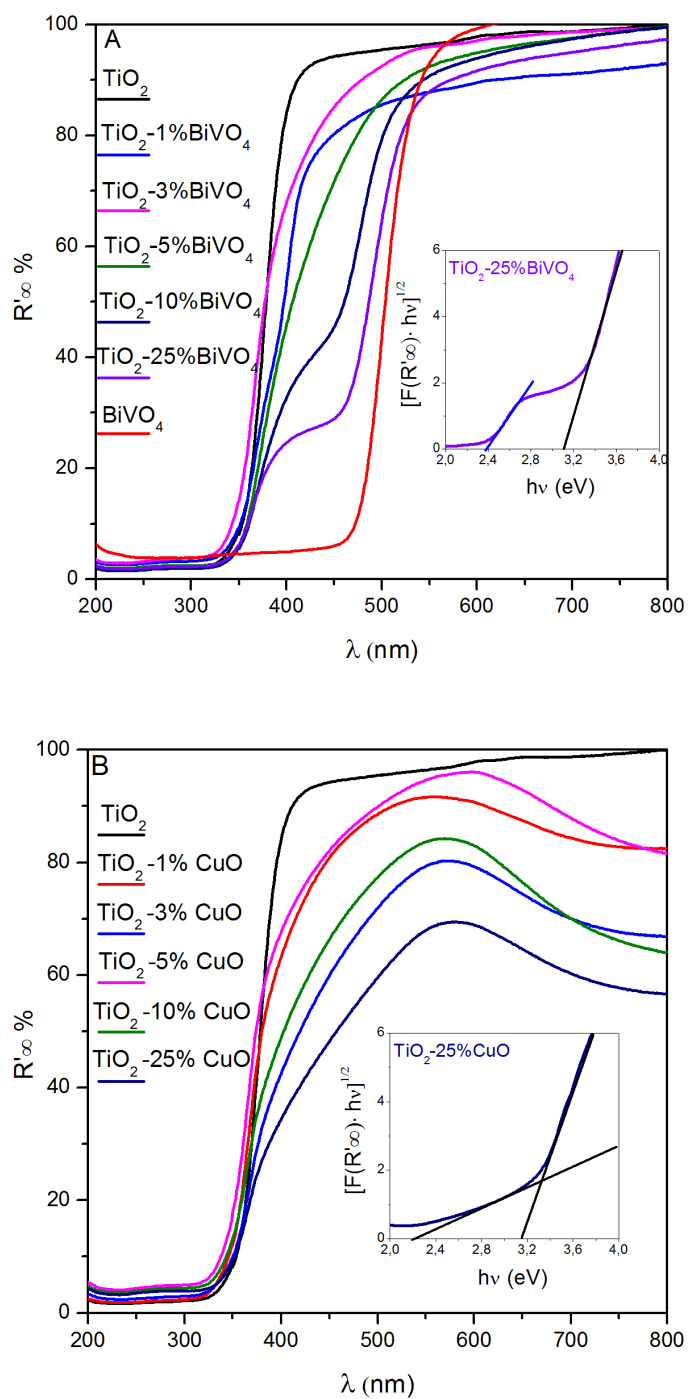
Fig. 1

**Fig. 2**





**Fig. 3**

**Fig. 4**

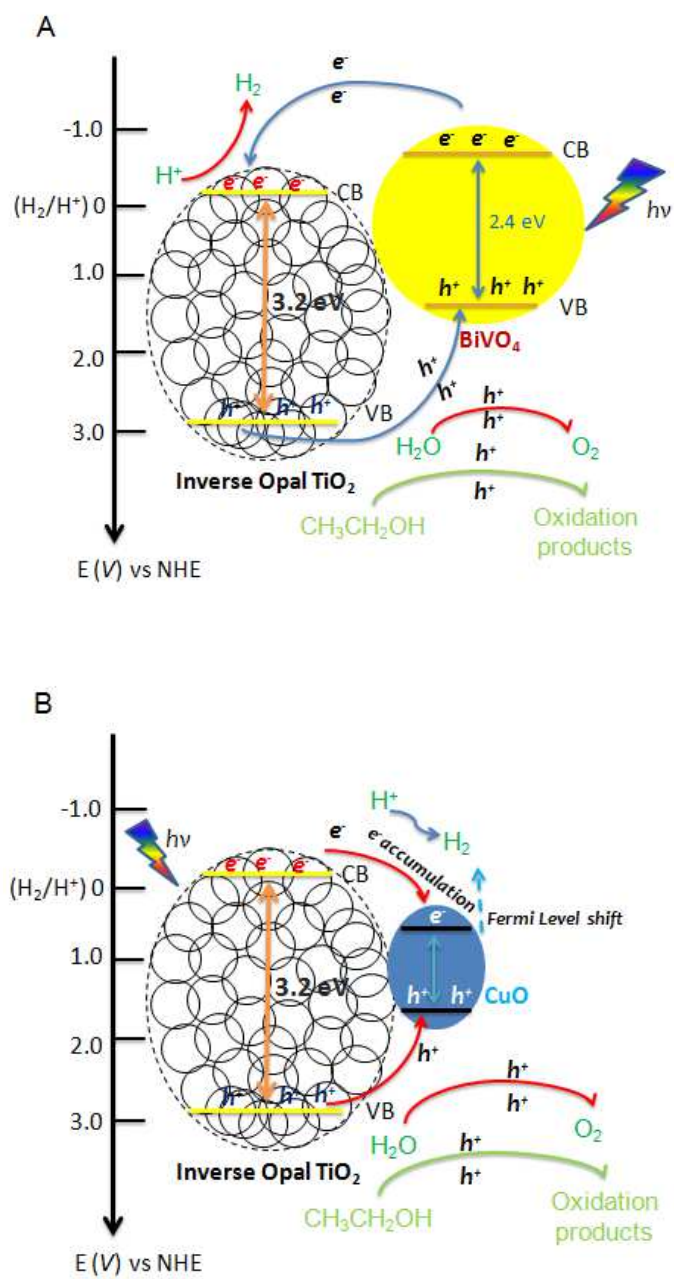


Fig. 5